ChemMedChem

ChemMedChem

Chemistry Europe
European Chemical Societies Publishing

RESEARCH ARTICLE OPEN ACCESS

Exploring 6-Hydroxy-3-Aryl/Heteroarylcoumarins as Promising Candidates Against *Trypanosoma cruzi*

C. N. Pereira[1,2] | L. da Silva Lara[3] | S. da Costa Lanera[3] | T. Pérez de Souza[3] | M. C. de Souza Pereira[3] | G. L. Delogu[4] | M. Silva dos Santos[1] | M. J. Matos[2]

[1]Laboratório de Síntese de Sistemas Heterocíclicos (LaSSH), Instituto de Física e Química (IFQ), Universidade Federal de Itajubá, Itajubá, Minas Gerais, Brazil | [2]Departamento de Química Orgánica, Facultade de Farmacia, Universidade Santiago de Compostela, Santiago de Compostela, Spain | [3]Laboratório de Ultraestrutura Celular, Instituto Oswaldo Cruz, Fiocruz, Rio de Janeiro, Brazil | [4]Department of Live and Environmental Sciences, University of Cagliari, Cittadella Universitaria, Monserrato, Italy

Correspondence: M. Silva dos Santos (mauriciosantos@unifei.edu.br) | M. J. Matos (mariajoao.correiapinto@usc.es)

Received: 22 January 2026 | **Revised:** 15 April 2026 | **Accepted:** 17 April 2026

Keywords: 2,3-dihydrobenzo[*b*][1,4]dioxine | chagas disease | coumarin scaffold | pyridine | *trypanosoma cruzi*

ABSTRACT

Chagas disease urgently requires the development of new, safe, and effective therapies. We evaluated a series of 6-hydroxy-3-aryl/heteroarylcoumarin derivatives against *Trypanosoma cruzi* to identify candidates with multistage activity. Our screening revealed that derivatives **1c** (2-pyridyl) and **1f** (2,3-dihydrobenzo[*b*][1,4]dioxine) are highly selective chemotypes toward trypomastigotes over Vero cells (SI = 549.45 and > 625, respectively), demonstrating submicromolar potency (IC_{50} = 0.91 and 0.80 μM, respectively), an activity up to 23-fold higher than benznidazole (Bz). The derivative **1f**, like Bz, also exhibited dual-stage activity, showing intracellular amastigote activity ($IC_{50} \sim 10$ μM). Mechanistic analysis using a washout assay revealed that, rather than eliminating intracellular forms, **1f** prevents the release of new trypomastigotes. Our findings suggest that **1f** targets the amastigote-to-trypomastigote differentiation pathway. The retention of a high intracellular parasitic load and the absence of trypomastigote release during the washout period strongly suggest that **1f** acts as a selective inhibitor of metacyclogenesis. This insight positions the coumarin scaffold bearing a 2,3-dihydrobenzo[*b*][1,4]dioxine substituent at position 3 as a promising starting point for developing improved multi-stage therapeutic candidates against *Trypanosoma cruzi*.

1 | Introduction

Chagas disease (CD), a vector-borne pathology caused by the protozoan *Trypanosoma cruzi* (*T. cruzi*), disproportionately affects populations in socioeconomically vulnerable conditions and is recognized by the World Health Organization (WHO) as a major neglected tropical disease (NTD) [1]. CD is endemic in 21 Latin American countries, with the highest prevalence in Bolivia, Argentina, Paraguay, Brazil, and Mexico. Historically, *T. cruzi* transmission in the endemic areas was mainly driven by contact with the feces of infected triatomine vectors ('kissing bugs'). However, additional routes, including congenital transmission, ingestion of contaminated food or beverages, blood transfusion, organ transplantation, and laboratory exposure, also play an important role in the disease's dissemination. Therefore, population mobility has contributed to its increasing detection in non-endemic regions, including the United States, Canada, Europe, Oceania, and Asia [2]. Current estimates indicate that approximately 6–7 million people are infected worldwide, resulting in about 12,000 deaths annually, and more than 100 million people reside in areas at risk of zoonotic transmission [1]. Beyond its substantial health burden, CD imposes significant socioeconomic consequences, including chronic morbidity, reduced productivity, and long-term healthcare expenditures [3]. Given its broad geographic distribution, chronic nature, and pronounced health

C. N. Pereira and L. da Silva Lara contributed equally to this work.

and socioeconomic impacts, CD remains a major public health challenge, emphasizing the urgent need for more effective therapeutic solutions.

CD unfolds in two distinct phases: an initial acute stage, typically presenting with mild or nonspecific symptoms such as fever, malaise, and localized swelling at the inoculation site, and a prolonged chronic stage that may remain clinically silent for years, yet can culminate in severe cardiac and gastrointestinal manifestations in a subset of patients [4]. Despite over five decades of research, current chemotherapy relies on only two nitro-functionalized heterocycles, benznidazole (Bz) and nifurtimox (Nfx), which are often poorly tolerated, require extended courses exceeding 2 months, and exhibit limited efficacy, particularly in chronic infections [5, 6]. To address these constraints, research has pursued alternative strategies, including drug repurposing, Bz alternative regimens, and the design of novel compounds targeting essential parasite survival targets. However, although several novel candidates have recently emerged, none has yet advanced to successful clinical application [7–9]. In some cases, shortening Bz treatment to 2 weeks and reducing the dose can retain similar efficacy to the standard 8-week treatment. However, in Brazilian cohorts, such Bz alternative regimens proved to be largely insufficient, revealing population-specific limitations of this combined strategy [10]. Repurposing fexinidazole, a drug developed for human African trypanosomiasis [11, 12], proved to be unviable for CD due to its poor tolerability at the therapeutic doses clinically evaluated [13]. These challenges underscore a critical unmet need: the discovery and development of innovative, safe, and effective agents that can target *T. cruzi* at different stages of the disease.

In recent years, our research group has focused on the synthesis and evaluation of trypanocidal activity in various heterocyclic systems. We have studied pyrazole-imidazolines [14–17], pyrazole-thiazolines [18], pyrazole-benzo[*d*]imidazoles [19], pyrazole-tetrahydropyrimidines [14, 20], pyrazole-thiadiazoles [21], and coumarins [22–26]. Regarding the coumarin scaffold, we identified 3-(3-bromophenyl)−6,7-dihydroxycoumarin (derivative **I**, Figure 1) as the most effective trypanocidal agent, with an IC_{50} of 33.6 ± 0.7 μM against the trypomastigote form of *T. cruzi*. This activity is comparable to that of the reference drug, Bz, which presented an IC_{50} of 20.0 ± 0.5 μM [22]. We also reported the synthesis of 7-hydroxy-3-nitrocoumarin-4-yl-nicotinate (derivative **II**, Figure 1), which effectively reduced the percentage of infected cells when evaluated against amastigote forms and outperformed the reference drug, Nfx [23]. The 7,8-dihydroxy-3-(2-hydroxyphenyl)coumarin (derivative **III**, Figure 1) showed a moderate peroxyl radical scavenging capacity (ORAC-FL = 2.23) and displayed remarkable selectivity for the epimastigote forms, achieving an IC_{50} of 1.31 ± 2.0 μM, significantly lower than Nfx's IC_{50} of 17.4 ± 1.3 μM [24]. *N*-(quinolin-3-yl)coumarin-3-carboxamide (derivative **IV**, Figure 1) showed high activity against the epimastigote stage, with an IC_{50} of 20.90 ± 0.01 μM, which is comparable to Nfx's IC_{50} of 17.40 ± 1.3 μM, while also exhibiting low cytotoxicity [25]. Finally, 3-amino-4-hydroxycoumarin (derivative **V**, Figure 1) showed good trypanocidal activity against the trypamastigote form, with an IC_{50} of 22.20 ± 2.1 μM and an ORAC-FL measurement of 4.36, similar to Nfx, which demonstrated, in the conditions of this study, an IC_{50} of 36.9 ± 3.4 μM [26].

Based on the previously outlined findings, we aimed to implement structural modifications to the coumarin scaffold at positions 3 and 6 to expand the chemical space and improve potential interactions with specific *T. cruzi* enzymes. In our search for novel trypanocidal agents, we synthesized and evaluated a series of 10 3-substituted-6-hydroxycoumarins **1(a-j).** Among the synthesized compounds, seven are being published for the first time: **1(a, b,e, f,h-j)**. The synthesis of **1(c, d,g)** has already been reported, but the trypanocidal activity was not evaluated beforehand [27–29]. These compounds were designed using the ring bioisosterism approach, replacing rings such as nicotinic, benzyl, and quinoline with various heterocycles while preserving the hydroxyl group at position 6, which is important for the coumarin scaffold's activity (Figure 1).

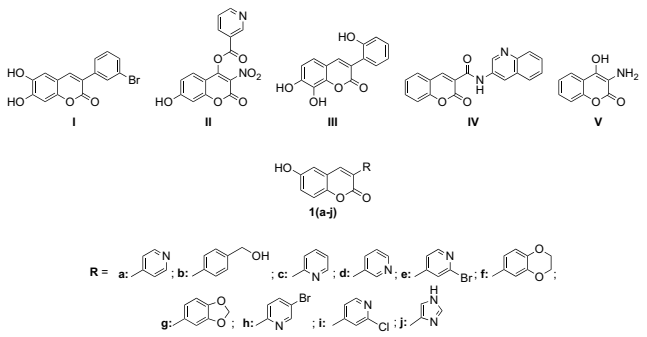

FIGURE 1 | Design strategy for the synthesized compounds based on a ring bioisosterism approach. Nicotinic, benzyl, and quinoline rings were replaced with various heterocycles while maintaining the hydroxyl group at position 6, a key feature for the biological activity of the coumarin scaffold.

2 | Results and Discussion

2.1 | Chemistry

Compounds **1(a-j)** were synthesized according to the synthetic pathway summarized in Scheme 1. Firstly, 2,5-dihydroxybenzaldehyde reacted with aryl/heteroarylacetic acids **2(a-j)**, through a Perkin-Oglialoro condensation, using potassium acetate (H_3CCO_2K) in acetic anhydride (Ac_2O), under reflux for 16 h, to achieve the key intermediates 6-acetoxy-3-aryl/heteroarylcoumarins **3(a-j)** in yields ranging from 11% to 72% [30]. The second step consists of a hydrolysis reaction of **3(a-j)**, utilizing aqueous hydrochloric acid (HCl) solution and methanol (MeOH), under reflux for 3 h, to attain the designed compounds **1(a-j)** in 47%-99% yields [30].

This synthetic strategy is highly efficient when free hydroxyl groups are present in the starting materials. The first step is corroborated by the appearance of a specific peak at low field in the ^{1}H NMR spectrum corresponding to H-4, which may indicate the closure of the coumarin ring. The second step of the reaction, deacylation, can then be confirmed by ^{1}H NMR, as evidenced by the absence of the methyl group peak (between 2 and 3 ppm) and the appearance of a new signal for the hydroxyl group (between 9 and 10 ppm).

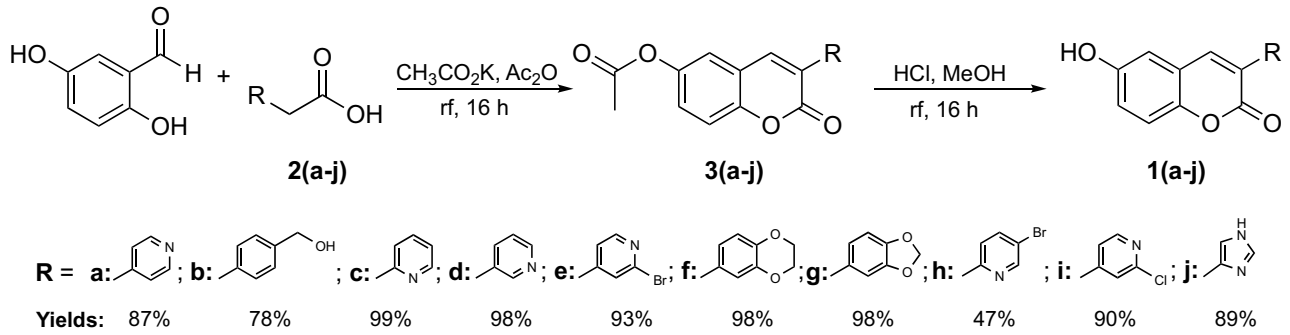

SCHEME 1 | Synthetic pathway to obtain the 6-hydroxy-3-aryl/heteroarylcoumarins **1(a-j)**.

2.2 | Biological Assays

The panel of newly synthesized 3-arylcoumarin derivatives **1(a–j)** was assessed for cytotoxicity and screened for anti-*T. cruzi* activity. Cytotoxic effects were evaluated in Vero cell monolayers after 24 and 72 hours of exposure. Coumarin derivatives exhibited low toxicity toward Vero cells (Table 1). After 24 h of exposure, all compounds showed CC_{50} values over 500 μM. When the incubation period was extended to 72 h to assess long-term toxicity, most derivatives exhibited $CC_{50} > 500$ μM, except for **1a** ($CC_{50} = 193.5 \pm 11.84$ μM), **1c** ($CC_{50} = 296.13 \pm 44.3$ μM), and **1g** ($CC_{50} = 476.63 \pm 33.04$ μM). The antiparasitic activity was evaluated using Vero cell monolayers and *T. cruzi* Dm28c expressing luciferase, which allowed the assessment of both parasite developmental stages, trypomastigotes and intracellular amastigotes, by exposing isolated parasites or infected cultures to compound concentrations ranging from 100 to 0.04 μM. Among the series, derivatives bearing 2-pyridyl (**1c**) and 2,3-dihydrobenzo[*b* [1, 4] dioxine (**1f**) as substituents at position 3 of the scaffold exhibited submicromolar activity against trypomastigotes, with IC_{50} values of 0.91 and 0.80 μM, respectively (Table 1). The 2-pyridyl derivative **1c** showed markedly enhanced activity compared with its isomeric analogs **1a** (4-pyridyl, $IC_{50} = 10.52 \pm 3.48$ μM) and **1d** (3-pyridyl, $IC_{50} > 100$ μM). This improved potency may be attributed to the stronger electronic influence of the nitrogen atom in the *ortho* position, which intensifies the inductive effect and modulates the electronic polarization of the coumarin scaffold. While the precise molecular target remains to be fully elucidated, the clear structure–activity relationship (SAR) patterns observed in this phenotypic screening, such as the activity drop upon introducing a bromine atom at position 3 into the 2-pyridyl ring (**1h**), or a chlorine at position 2 into the 4-pyridyl derivative (**1i**) (Table 1), provide valuable insights into the chemical requirements for anti-*T. cruzi* activity. Strikingly, derivatives **1c** and **1f** exhibited substantially higher potency against trypomastigotes than Bz, with approximately 20- to 23-fold higher activity and markedly improved selectivity, yielding selectivity indices (SI) of 549.45 and > 625, respectively, compared with 26.42 for Bz. Additionally, derivative **1f** also inhibited intracellular amastigotes, with an IC_{50} of 10.20 ± 0.79 μM and a SI > 49.02. Few derivatives achieved IC_{90} values below 100 μM. Derivatives **1a**, **1c**, and **1f** showed IC_{90} values around 30 μM against trypomastigotes, while **1a** and **1f** had IC_{90} values of 72.81 and 28.36 μM against intracellular amastigotes, respectively (Table 1). Although **1f** was less potent

TABLE 1 | Anti-*T. cruzi* activity and toxicity profiles of the studied compounds **1(a-j)**.

	Anti-*T. cruzi* activity						
	Trypomastigotes			Intracellular amastigotes			Cytotoxicity
Cmp	IC_{50}, μM	IC_{90}, μM	SI[b]	IC_{50}, μM	IC_{90}, μM	SI	CC_{50}/72h, μM[a]
1a	10.52 ± 3.48	30.75 ± 1.94	>47.52	23.93 ± 1.13	72.81 ± 2.89	8.08	193.5 ± 11.84
1b	10.43 ± 2.62	>100	>47.93	74.05 ± 2.31	>100	6.75	>500
1c	0.91 ± 0.02	30.15 ± 3.94	>549.45	>100	>100	ND	296.13 ± 44.3
1d	>100	>100	ND	>100	>100	ND	>500
1e	>100	>100	ND	>100	>100	ND	>500
1f	0.80 ± 0.15	30.67 ± 1.38	>625	10.20 ± 0.79	28.36 ± 3.65	>49.02	>500
1g	46.97 ± 5.94	>100	>10.64	29.95 ± 1.57	>100	15.91	476.63 ± 33.04
1h	>100	>100	ND	>100	>100	ND	>500
1i	>100	>100	ND	>100	>100	ND	>500
1j	>100	>100	ND	>100	>100	ND	>500
Bz	18.92 ± 1.97	>100	>26.42	3.77 ± 1.03	12.21 ± 2.64	>132.62	>500

Note: Mean IC_{50} and IC_{90} values obtained from three independent experiments ± standard deviation (SD). Compound: Cmp; IC_{50}: concentration required to inhibit parasite viability by 50%. CC_{50}: concentration that reduces Vero cell viability by 50%.

[a]CC_{50} determined after 72 h of incubation (CC_{50}/72 h). All compounds exhibited $CC_{50} > 500$ μM at 24 h.

[b]Selectivity Index (SI) for trypomastigotes calculated as CC_{50} (24 h)/IC_{50}. SI for amastigotes calculated as CC_{50} (72 h)/IC_{50}.

than Bz ($IC_{50} = 3.77 \pm 1.03\ \mu M$) against amastigotes, it also exhibited a dual-stage profile, capable of targeting both circulating and intracellular forms of *T. cruzi* with high selectivity, underscoring the potential of the coumarin scaffold as an interesting antiparasitic chemotype.

Given the activity of **1f** against both developmental stages, this derivative was selected for a washout assay to further evaluate its trypanocidal potential. The washout assay assesses in vitro sterility by monitoring parasite recurrence after compound withdrawal. This evaluation has gained particular importance in light of the therapeutic failure of posaconazole [31, 32], which was later shown to be unable to prevent parasite relapse in vitro, even after prolonged treatment periods [33]. *T. cruzi* can give rise to persister-like cells that withstand strong drug pressure for extended periods and quickly rebound once the compound is removed, representing a major challenge for achieving a sterile cure [34].

Thus, the assay serves as a critical tool for discriminating between parasiticidal and merely parasitostatic effects of drug candidates. Then, *T. cruzi*-infected Vero cells were treated for 10 days, followed by an additional 10-day period without compound exposure. Both concentrations of **1f** (28 and 56 μM) significantly reduced the release of trypomastigote into the culture supernatant, exhibiting an inhibition profile comparable to that of Bz (Figure 2). However, **1f** failed to eliminate intracellular parasites, maintaining a parasitic load similar to that of untreated infected cultures, whereas Bz (100 μM) significantly reduced the intracellular burden (Figure 2). The simultaneous retention of high intracellular parasite load and the absence of trypomastigote release suggest that **1f** interferes with the intracellular differentiation of amastigotes into trypomastigotes, rather than promoting parasite clearance. Thus, understanding the specific pathways targeted during differentiation may be essential for optimizing this scaffold and enhancing its curative potential.

The activity of coumarin derivatives against *T. cruzi* aligns with the amount of evidence supporting coumarins as versatile antitrypanosomal agents. Studies on natural coumarins, including mammea-type compounds, calanolides, and chalepin derivatives, have revealed multiple mechanisms of action, including disruption of parasite membranes, mitochondrial swelling, nuclear damage, and selective inhibition of key glycolytic enzymes, such as glycosomal GAPDH [35]. Coumarin-chalcone hybrids demonstrated significant activity and selectivity against intracellular amastigotes of *T. cruzi* and *Leishmania braziliensis*. Molecular docking studies revealed that the most active compound exhibited high affinity for trypanothione reductase, establishing multiple interactions with the active site [36]. Additional mechanisms, including oxidative stress induction and the inhibition of cysteine proteases, have also been reported for coumarin-based molecules [37]. This variety of mechanisms of action reported in synthetic and natural coumarin derivatives suggests that these compounds may interact with multiple targets in the parasite. Previous studies indicate that this multifactorial characteristic may enhance therapeutic efficacy and decrease the likelihood of *T. cruzi* resistance, a limitation frequently associated with single-target drugs [38].

As previously reported and consistent with our findings, nitrocoumarins bearing nitrogen-rich heterocycles, particularly pyridine, have been highlighted as promising trypanocidal agents, suggesting inhibition of enzymes essential for parasite survival [23]. The notable selectivity of derivatives **1c** and **1f** for the trypomastigote form suggests that distinct physiological features of the parasite stages may be involved. Trypomastigotes have a high metabolic rate and energy expenditure due to their intense motility, making them highly sensitive to inhibition of key glycolytic enzymes (e.g., glycosomal GAPDH, a target of coumarins), which leads to rapid energy depletion. In contrast, the amastigote, adapted for intracellular replication, uses different energy sources and exhibits greater plasticity, thereby enabling it to withstand energy stress. The differential activity of **1f** against trypomastigotes and amastigotes, however, is strongly supported by the distinct energy acquisition strategies employed by these forms. While bloodstream trypomastigotes live in a glucose-rich environment and rely heavily on glycolysis for their high energy demands, the intracellular amastigote drastically reduces the expression of

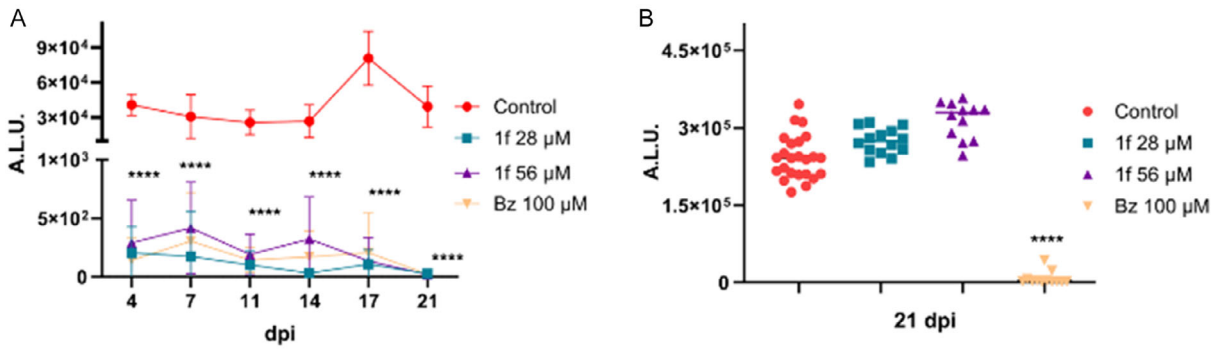

FIGURE 2 | Evaluation of the in vitro reversibility of the derivative **1f** and Bz in Vero cell cultures infected with *T. cruzi*. Cells were exposed to concentrations corresponding to 28 μM (IC_{90}) and 56 μM ($2 \times IC_{90}$) of derivative **1f** or 100 μM of Bz for 10 days, followed by an additional 10-day period in drug-free medium. (A) Treatment with **1f** significantly reduced the release of trypomastigote forms in the supernatant during the 21 days post-infection (dpi), similarly to treatment with Bz. (B) However, compound **1f** could not eliminate intracellular parasites, maintaining levels comparable to the untreated infected group. In contrast, Bz promoted a significant decrease in intracellular load. Parasite viability was determined by luciferase activity, expressed in Arbitrary Luminescence Units (A.L.U.). The results represent the average of three independent experiments. Statistical analysis was performed using one-way ANOVA, followed by Tukey's post-hoc test. (****) indicates a statistically significant difference compared to the untreated control, with $p \leq 0.0001$.

hexose transporter (TcHT) proteins [39]. Consequently, amastigote primarily shifts its metabolism to utilize amino acids and fatty acids scavenged from the host cell [40]. This metabolic independence from glucose-dependent glycolysis renders the amastigote less vulnerable to rapid energy depletion induced by derivative **1f**, complementing the challenge posed by the host cell permeability barrier.

Together, these findings reinforce that rationally designed synthetic 3-aryl/heteroarylcoumarins, such as those evaluated here, may engage similar molecular targets or pathways, offering opportunities to improve potency and selectivity through strategic structural optimization. Overall, these insights support the scaffold's potential as a promising chemotype for developing selective and effective therapeutic candidates for CD.

3 | Conclusion

In summary, this study validates the strategy of modifying the coumarin scaffold with heteroaryl substituents at position 3. The derivative **1f**, along with **1c**, stands out for its high submicromolar potency and superior selectivity against the infective trypomastigote form, an activity profile consistent with the high energy demand of this parasite stage. Derivative **1f**, in particular, demonstrated valuable dual activity, shared with benznidazole. Furthermore, the washout assay with this molecule revealed a peculiar property, a possible inhibition of parasite differentiation (amastigote-to-trypomastigote). This mechanism suggests a new mode of action for this class of compounds, warranting further exploration. Accordingly, the development priority is rational drug design to enhance amastigote-parasiticidal potency, with the aim of developing improved multi-stage therapeutic candidates for CD.

4 | Experimental Section

4.1 | Chemistry

4.1.1 | General information

The starting materials and reagents were obtained from commercial suppliers (Sigma–Aldrich) and were used without further purification. Melting points (Mp) are uncorrected and were determined using a Reichert Kofler Thermopan or in capillary tubes in a Büchi 510 apparatus. ^{1}H NMR (250 MHz) and ^{13}C NMR (63 MHz) spectra were recorded on a Bruker AMX spectrometer. ^{1}H NMR (300 MHz) and ^{13}C NMR (75.4 MHz) spectra were recorded on a Varian Mercury 300. ^{1}H NMR (500 MHz) and ^{13}C NMR (126 MHz) spectra were recorded on a Bruker DRX-500. The spectra were obtained using $CDCl_3$ or DMSO-$_{d6}$ as solvent. Chemical shifts (δ) are expressed in parts per million (ppm) using tetramethylsilane (TMS) as an internal standard. Coupling constants *J* are expressed in Hertz (Hz). Spin multiplicities are given as s (singlet), d (doublet), dd (doublet of doublets), ddd (doublet of doublets of doublets), t (triplet), td (triplet of doublets), and m (multiplet). The analytical results document > 95% purity for all compounds. Flash chromatography (FC) was performed on silica gel (Merck 60, 230– 400 mesh). The progress of the reactions was monitored by TLC, which was performed on precoated silica gel plates (Merck 60 F254).

4.1.2 | General procedure for the synthesis of 6-acetoxy-3-aryl/heteroarylcoumarins 3(a-j)

Acetoxylated coumarins **3(a-j)** were synthesized under anhydrous conditions, using equipment previously dried at 60°C for at least 12 h and also at 300°C for a few minutes immediately before use. The solution containing anhydrous H_3CCO_2K (2.94 mmol), the appropriate phenylacetic acid derivative **2(a-j)** (1.67 mmol), and 2,5-dihydroxybenzaldehyde (1.67 mmol) in Ac_2O (1.2 mL) was refluxed (138°C) with stirring for 16 h. The reaction mixture was cooled, neutralized with 10% aqueous $NaHCO_3$ solution, and extracted (3 x 30 mL) with ethyl acetate (AcOEt). The organic layers were pooled, washed with distilled water, dried (anhydrous Na_2SO_4), filtered, and evaporated under reduced pressure. The products were purified by flash column chromatography using isohexane/EtOAc 9:1 as the mobile phase and Merck 60, 230–400 silica gel as the stationary phase, and dried.

4.1.3 | 6-Acetoxy-3-(pyridin-4-yl)coumarin (3a)

Yield: 11%. M.P.: 130°C-132°C. ^{1}H NMR (250 MHz, $CDCl_3$) δ (ppm) *J* (Hz): 8.57 (d, $J = 6.1$, 2H), 7.40–7.22 (m, 3H), 7.11–6.99 (m, 3H), 2.33 (s, 3H, CH_3). ^{13}C NMR (63 MHz, DMSO-d_6) δ (ppm): 169.1, 165.6, 152.8, 149.5, 145.7, 142.1, 141.0, 128.8, 125.9, 123.7, 122.5, 121.0, 119.3, 20.9.

4.1.4 | 6-Acetoxy-3-(4-hydroxymethyl)phenyl) coumarin (3b)

Yield: 38%. M.P.: 113°C–114°C. ^{1}H NMR (250 MHz, $CDCl_3$) δ (ppm) *J* (Hz): 7.76 (s, 1H); 7.45 (d, $J = 8.5$, 2H); 7.37 (d, $J = 8.1$, 1H), 7.32 (d, $J = 2.6$, 1H), 7.24 (dd, $J = 8.1$, 2.6, 1H), 7.00 (d, $J = 8.5$, 2H), 5.15 (s, 2H, CH_2), 2.35 (s, 3H, CH_3), 2.13 (s, 3H, CH_3). ^{13}C NMR (63 MHz, $CDCl_3$) δ (ppm): 169.1, 165.6, 152.8, 149.5, 145.7, 142.1, 141.0, 128.8, 125.9, 123.7, 122.5, 121.0, 119.3, 20.9.

4.1.5 | 6-Acetoxy-3-(pyridin-2-yl)coumarin (3c)

Yield: 32%. M.P.: 128°C-130°C. ^{1}H NMR (250 MHz, $CDCl_3$) δ (ppm) *J* (Hz): 8.70 (s, 1H), 8.66 (dd, $J = 4.9$, 1.6, 1H), 8.39 (d, $J = 8.1$, 1H), 7.76 (td, $J = 8.1$, 1.6, 1H), 7.31–7.38 (m, 2H), 7.30–7.22 (m, 2H), 2.31 (s, 3H, CH_3). ^{13}C NMR (63 MHz, $CDCl_3$) δ (ppm): 169.8, 157.0, 151.2, 150.8, 149.3, 146.6, 145.1, 141.5, 136.6, 125.6, 124.0, 123.5, 120.7, 119.8, 117.2, 20.9.

4.1.6 | 6-Acetoxy-3-(pyridin-3-yl)coumarin (3d)

Yield: 61%. M.P.: 166°C-168°C. ^{1}H NMR (250 MHz, $CDCl_3$) δ (ppm) *J* (Hz): 8.83 (d, $J = 1.6$, 1H), 8.63 (dd, $J = 4.9$, 1.6, 1H), 8.10 (ddd, $J = 8.0$, 2.4, 1.6, 1H), 7.81 (s, 1H), 7.41–7.31 (m, 3H), 7.28 (d, $J = 2.7$, 1H), 2.32 (s, 3H, CH_3). ^{13}C NMR (63 MHz, $CDCl_3$) δ (ppm): 169.1, 159.8, 153.6, 151.0, 149., 148.8, 146.8, 139.6, 136.1, 130.3, 125.9, 125.4, 123.0, 120.2, 119.5, 117.5, 20.9.

4.1.7 | 6-Acetoxy-3-(2-bromopyridin-4-yl)coumarin (3e)

Yield: 72%. M.P.: 132°C–134°C. ^{1}H NMR (250 MHz, $CDCl_3$) δ (ppm) *J* (Hz): 8.43 (d, $J = 5.2$, 1H), 7.89 (s, 1H), 7.82 (d, $J = 1.6$, 1H), 7.61 (dd, $J = 5.2$, 1.6, 1H), 7.40–7.28 (m, 3H), 2.32 (s, 3H, CH_3). ^{13}C RMN (63 MHz, $CDCl_3$) δ (ppm): 173.5,

165.2, 151.1, 150.1, 146.8, 144.3, 142.5, 141.2, 126.7, 126.4, 126.3, 121.7, 120.5, 118.9, 117.6, 20.8.

4.1.8 | 6-Acetoxy-3-(2,3-dihydrobenzo[b [1, 4] dioxin-6-yl) coumarin (3f)

Yield: 52%. M.P.: 122°C–124°C. ^{1}H NMR (250 MHz, $CDCl_3$) δ (ppm) *J* (Hz): 8.13 (s, 1H), 7.49 (d, *J* = 2.6), 7.43 (d, *J* = 8.9, 1H), 7.33 (dd, *J* = 8.9, 2.6, 1H), 7.25 (d, *J* = 2.0, 1H), 7.22 (dd, *J* = 8.4, 2.0, 1H), 6.90 (d, *J* = 8.4, 1H), 4.25 (s, 4H, 2xCH_2), 2.27 (s, 3H, CH_3). ^{13}C NMR (63 MHz, $CDCl_3$) δ (ppm): 169.1, 164.0, 150.6, 146.6, 144.4, 143.2, 137.8, 128.3, 127.5, 124.4, 121.7, 120.0, 119.7, 117.5, 117.2, 117.2, 64.4, 64.2, 20.9.

4.1.9 | 6-Acetoxy-3-(benzo[d [1, 3] dioxol-5-yl) coumarin (3g)

Yield: 42%. M.P.: 172°C–174°C. ^{1}H NMR (250 MHz, $CDCl_3$) δ (ppm) *J* (Hz): 7.67 (s, 1H), 7.34 (d, *J* = 8.8, 1H), 7.26 (d, *J* = 2.6, 1H), 7.22–7.16 (m, 2H), 7.14 (d, *J* = 1.8, 1H), 6.86 (d, *J* = 8.0, 1H), 5.99 (s, 2H, CH_2), 2.31 (s, 3H, CH_3). ^{13}C NMR (63 MHz, $CDCl_3$) δ (ppm): 169.2, 167.6, 150.6, 148.3, 147.6, 146.6, 138.0, 128.5, 128.1, 124.5, 122.5, 120.0, 119.8, 117.3, 108.9, 108.2, 101.3, 20.9.

4.1.10 | 6-Acetoxy-3-(5-bromopyridin-2-yl)coumarin (3h)

Yield: 15%. M.P.: 170°C–172°C. ^{1}H NMR (250 MHz, $CDCl_3$) δ (ppm) *J* (Hz): 7.79 (s, 1H), 7.73 (s, 1H), 7.36–7.34 (m, 2H), 7.23 (d, *J* = 1.6, 1H), 6.43–6.36 (m, 2H), 2.29 (s, 3H, CH_3). ^{13}C NMR (63 MHz, $CDCl_3$) δ (ppm): 166.0, 164.2, 154.7, 153.6, 147.0, 143.4, 141.8, 134.5, 122.8, 120.8, 119.7, 119.2, 115.5, 115.2, 16.1.

4.1.11 | 6-Acetoxy-3-(2-chloropyridin-4-yl)coumarin (3i)

Yield: 59%. M.P.: 166°C–168°C.^{1}H NMR (300 MHz, $CDCl_3$) δ (ppm) *J* (Hz): 8.49 (dd, *J* = 5.3, 0.7, 1H), 7.94 (s, 1H), 7.72 (dd, *J* = 1.6, 0.7, 1H), 7.61 (dd, *J* = 5.2, 1.6, 1H), 7.43–7.32 (m, 3H), 2.36 (s, 3H, CH_3). ^{13}C NMR (75 MHz, $CDCl_3$) δ (ppm): 171.7, 158.6, 151.9, 151.1, 149.7, 144.6, 141.2, 127.8, 126.3, 124.9, 123.1, 121.3, 120.5, 118.9, 117.6, 20.8.

4.1.12 | 6-Acetoxy-3-(1H-imidazol-4-yl)coumarin (3j)

Yield: 31%. M.P.: 210°C–212°C. ^{1}H NMR (300 MHz, $CDCl_3$) δ (ppm) *J* (Hz): 9.46 (s, 1H, NH), 8.57 (s, 1H), 8.37 (s, 1H), 8.32 (s, 1H), 7.40–7.18 (m, 3H), 2.37 (s, 3H, CH_3). ^{13}C NMR (75.4 MHz, $CDCl_3$) δ (ppm): 168.9, 156.4, 155.8, 151.3, 146.6, 144.5, 144.0, 141.7, 139.4, 136.8, 126.1, 120.4, 110.5, 23.0.

4.1.13 | General procedure for the synthesis of 6-hydroxy-3-aryl/heteroarylcoumarins 1(a-j)

The key intermediate **3(a-j)** (0.003 mol) reacted with 6.5 mL of 2 mol L^{-1} aqueous HCl solution, using 2 mL of methanol as solvent. The mixture was refluxed for 3 h with magnetic stirring. After that, the resulting reaction mixture was cooled in an ice bath. The solid isolated was filtered, washed with cold distilled water, and dried under vacuum, to achieve the desired compounds **1(a-j)**.

4.1.14 | 6-Hydroxy-3-(pyridin-4-yl)coumarin (1a)

Yield: 87%. M.P.: 240°C–242°C. ^{1}H NMR (250 MHz, DMSO-$_{d6}$) δ (ppm) *J* (Hz): 9.73 (s, 1H, OH), 8.72 (d, *J* = 6.8, 2H, H-2′, H-6′), 8.10 (d, *J* = 6.8, 2H, H-3′, H-5′), 7.95 (d, *J* = 8.4, 1H, H-8), 7.35 (d, *J* = 8.4, 1H, H-7), 7.02 (d, *J* = 2.7, 1H, H-5), 6.72 (s, 1H, H-4). ^{13}C (63 MHz, DMSO-$_{d6}$) δ (ppm): 168.3, 154.5, 150.2, 150.1, 141.3, 136.2, 123.1, 122.2, 120.1, 119.6, 117.3, 113.3.

4.1.15 | 6-Hydroxy-3-(4-hydroxymethyl)phenyl) coumarin (1b)

Yield: 78%. M.P.: 113°C–114°C. ^{1}H NMR (250 MHz, DMSO-$_{d6}$) δ (ppm) *J* (Hz): 9.76 (s, 1H, OH), 8.16 (s, 1H, H-4), 7.69 (d, *J* = 7.9, 2H, H-2′, H-6′), 7.40 (d, *J* = 7.9, 2H, H-3′, H-5′), 7.28 (d, *J* = 8.8, 1H, H-8), 7.10 (d, *J* = 2.9, 1H, H-5), 7.04 (dd, *J* = 8.8, 2.9, 1H, H-7), 5.27 (t, *J* = 5.7, 1H, OH), 4.55 (d, *J* = 5.7, 2H, 2xHa). ^{13}C NMR (300 MHz, DMSO-$_{d6}$) δ (ppm): 154.0, 146.4, 143.1, 140.3, 133.3, 128.4, 126.9, 126.3, 120.2, 119.8, 116.8, 116.8, 112.6, 62.7.

4.1.16 | 6-Hydroxy-3-(pyridin-2-yl)coumarin (1c)

Yield: 99%. M.P.: 236°C-238°C. ^{1}H NMR (300 MHz, DMSO-$_{d6}$) δ (ppm) *J* (Hz): 8.81 (s, 2H, H-4, H-5), 8.36 (d, *J* = 8.0, 1H, H-8), 8.20 (t, *J* = 7.7, 1H, H-4′), 7.68 (t, *J* = 7.7, 1H, H-5′), 7.37 (d, *J* = 8.0, 1H, H-7), 7.25–7.17 (m, 2H, H-3′, H-6′), 4.70 (s, 1H, OH). ^{13}C NMR (75 MHz, DMSO-$_{d6}$) δ (ppm): 159.8, 154.7, 154.3, 150.0, 147.4, 144.6, 140.5, 125.3, 125.1, 122.8, 122.0, 119.8, 117.5, 113.8.

4.1.17 | 6-Hydroxy-3-(pyridin-3-yl)coumarin (1d)

Yield: 98%. M.P.: 288°C-290°C. ^{1}H NMR (250 MHz, DMSO-$_{d6}$) δ (ppm) *J* (Hz): 9.88 (s, 1H, OH), 9.00 (s, 1H, H-2′), 8.69 (d, *J* = 5.1, 1H, H-6′), 8.41 (d, *J* = 7.3, 1H, H-4′), 8.37 (s, 1H, H-4), 7.71 (dd, *J* = 7.3, 5.1, 1H, H-5′), 7.28 (d, *J* = 8.6, 1H, H-8), 7.09 (s, 1H, H-5), 7.06 (d, *J* = 8.6, 1H, H-7). ^{13}C NMR (63 MHz, DMSO-$_{d6}$) δ (ppm): 164.4, 154.2, 148.0, 146.4, 146.3, 142.4, 132.1, 132.1, 124.6, 123.0, 120.8, 119.8, 117.1, 112.9.

4.1.18 | 3-(2-Bromopyridin-4-yl)-6-hydroxycoumarin (1e)

Yield: 93%. M.P.: 266°C–268°C. ^{1}H NMR (250 MHz, DMSO-$_{d6}$) δ (ppm) *J* (Hz): (s, 1H, H-4), 8.43 (dd, *J* = 5.2, 0.8, 1H, H-6′), 8.00 (dd, *J* = 1.7, 0.8, 1H, H-3′), 7.80 (dd, *J* = 5.2, 1.7, 1H, H-5′), 7.30–7.26 (m, 1H, H-8), 7.10–7.06 (m, 2H, H-5, H-7), 4.10 (s, 1H, OH). ^{13}C NMR (63 mHz, DMSO-$_{d6}$) δ (ppm): 161.5, 155.9, 154.2, 150.5, 146.9, 143.6, 141.7, 126.8, 122.7, 122.6, 121.3, 119.6, 117.1, 113.1.

4.1.19 | 3-(2,3-Dihydrobenzo[b [1, 4] dioxin-6-yl)-6-hydroxycoumarin (1f)

Yield: 98%. M.P.: 230°C–232°C. ^{1}H NMR (250 MHz, DMSO-$_{d6}$) δ (ppm) *J* (Hz): 9.71 (s, 1H, OH), 8.07 (s, 1H, H-4), 7.25–7.17 (m, 3H, H-5′, H-7′, H-8′), 7.03 (d, *J* = 2.9, 1H, H-5), 6.97 (dd, *J* = 8.4, 2.9, 1H, H-7), 6.89 (d, *J* = 8.4, 1H, H-8), 4.24 (s, 4H, 2xH-2′, 2xH-3′). ^{13}C NMR (63 MHz, DMSO-$_{d6}$) δ (ppm): 160.0, 153.9, 146.3, 144.0, 143.0, 139.6, 127.9, 126.2, 121.7, 120.2, 119.6, 117.4, 116.9, 116.8, 112.6, 64.4, 64.1.

4.1.20 | 3-(Benzo[d [1, 3] dioxol-5-yl)-6-hydroxycoumarin (1g)

Yield: 98%. M.P.: 222°C–224°C. ^{1}H NMR (500 MHz, DMSO-$_{d6}$) δ (ppm) *J* (Hz): 9.73 (s, 1H, OH), 8.11 (s, 1H, H-4), 7.30 (d, *J* = 1.8, 1H, H-4′), 7.26 (dd, *J* = 8.3, 1.8, 2H, H-8, H-6′), 7.08 (d, *J* = 2.8, 1H, H-5), 7.04–6.99 (m, 2H, H-7, H-7′), 6.08 (s, 2H, 2xH-2′). ^{13}C NMR (125 MHz, DMSO-$_{d6}$) δ (ppm): 160.4, 154.3, 148.0, 147.6, 146.6, 140.1, 129.1, 126.8, 123.0, 120.5, 120.0, 117.1, 112.9, 109.3, 108.5, 101.8.

4.1.21 | 3-(5-Bromopyridin-2-yl)-6-hydroxycoumarin (1h)

Yield: 47%. M.P.: 250°C–252°C. ^{1}H NMR (250 MHz, DMSO-$_{d6}$) δ (ppm) *J* (Hz): 9.72 (s, 1H, OH), 7.94 (d, *J* = 9.6, 1H, H-8), 7.22–7.18 (m, 1H, H-4′), 7.08–6.71 (m, 4H, H-4, H-5, H-3′, H-6′), 6.39 (dd, *J* = 9.5, 1.3, 1H, H-7).^{13}C NMR (63 MHz, DMSO-$_{d6}$) δ (ppm): 160.4, 154.1, 153.9, 150.1, 146.9, 144.3, 132.1, 124.6, 120.0, 119.4, 118.4, 117.3, 116.4, 112.6.

4.1.22 | 3-(2-Chloropyridin-4-yl)-6-hydroxycoumarin (1i)

Yield: 90%. M.P.: 280°C–282°C. ^{1}H NMR (250 MHz, DMSO-$_{d6}$) δ (ppm) *J* (Hz): 9.87 (s, 1H, OH), 8.51 (s, 1H, H-4), 8.50 (d, *J* = 5.1, 1H, H-6′), 7.91 (s, 1H, H-3′), 7.82 (d, *J* = 5.1, 1H, H-5′), 7.32 (d, *J* = 8.4, 1H, H-8), 7.13–7.11 (m, 2H, H-5, H-7). ^{13}C NMR (63 MHz, DMSO-$_{d6}$) δ (ppm): 159.6, 154.5, 151.0, 150.4, 147.3, 146.3, 144.0, 123.5, 123.2, 122.7, 121.7, 119.9, 117.5, 113.5.

4.1.23 | 6-Hydroxy-3-(1H-imidazol-4-yl)coumarin (1j)

Yield: 89%. M.P.: 346°C–348°C. ^{1}H NMR (500 MHz, DMSO-$_{d6}$) δ (ppm) *J* (Hz): 12.32 (s, 1H, NH), 9.68 (s, 1H, OH), 8.45 (s, 1H, H-4), 7.81 (s, 1H, H-2′), 7.80 (s, 1H, H-5′), 7.26 (d, *J* = 8.8, 1H, H-8), 7.13 (d, *J* = 2.8, 1H, H-5), 6.99 (dd, *J* = 8.8, 2.8, 1H, H-7). ^{13}C NMR (125 MHz, DMSO-$_{d6}$) δ (ppm): 159.7, 154.4, 145.9, 136.7, 134.7 134.1, 121.7, 120.6, 119.2, 117.8, 117.1, 112.7.

4.2 | Cell culture

Vero cells (BCRJ code 0245), obtained from the Rio de Janeiro Cell Bank, were cultured in RPMI-1640 medium supplemented with 10% fetal bovine serum (FBS) and 1 mM L-glutamine, and maintained at 37ºC in a humidified 5% CO_2 atmosphere. Confluent monolayers were dissociated weekly using 0.025% trypsin-EDTA solution, and cells were seeded into 96-well plates or flasks as required. Vero cells were used for phenotypic screening assays, the washout assay, and the isolation of trypomastigote forms of *T. cruzi*.

4.3 | Trypanosoma cruzi

Genetically modified *T. cruzi* parasites, specifically the Dm28c clone (TcI) expressing the firefly luciferase gene (Dm28c-Luc), were kindly provided by Dr. Cristina Henriques [41]. The Dm28c-Luc was maintained in Vero cells using RPMI 1640 medium supplemented with 10% FBS. At 4 days post-infection (dpi), trypomastigotes released into the culture supernatant were harvested, centrifuged (4000 rpm, 20 min, 4°C), and quantified with a Neubauer chamber. These trypomastigotes were used in phenotypic screening assays to evaluate antiparasitic activity [18].

4.4 | Cytotoxicity assay

Vero cells were used to evaluate the toxicity effect of coumarin analogs and Bz. The cells were cultured in 96-well plates (1.5×10^4 cells/well) and after 24 h of seeding, were treated for 24 and 72 h at 37ºC with coumarin analogs or Bz at concentrations ranging from 15.62–500 μM. Cell viability was determined by measuring ATP levels using the CellTiter-Glo kit (Promega Corporation, Madison, WI, USA), followed by luminescence detection on the Glomax microplate reader (Promega Corporation, Madison, WI, USA). The concentration that reduced cell viability by 50% (CC_{50}) was calculated using GraphPad Prism software (version 8.0). Dimethyl sulfoxide (DMSO) was used as a solvent in all experimental groups at low concentrations (≤1%). At least three independent experiments were performed in duplicate.

4.5 | Anti-T. cruzi in vitro assay

Phenotypic screening of the coumarin derivatives was performed using *T. cruzi* Dm28c-Luc. Both trypomastigotes and amastigote forms were evaluated using a luminescence assay. Trypomastigotes (1×10^6 parasites/well) were exposed to coumarin derivatives or Bz at concentrations ranging from 0.41 to 100 μM for 24 h at 37°C in white 96-well plates with clear bottoms. To assess the effect of coumarin against intracellular amastigotes, Vero cells (1.5×10^4 cells/well) were seeded in a white 96-well plate with a clear bottom and infected with *T. cruzi* Dm28c-Luc at a 10:1 parasite-to-host cell ratio for 24 h. Infected cultures were treated for 72 h at 37ºC with different concentrations of coumarin derivatives (0.41–100 μM). Following incubation, D-luciferin solution (300 μg/mL) was added to assess parasite viability by measuring luminescence with a Glomax-Multi Detection microplate reader (Promega Corporation, Madison, WI, USA). The IC_{50} and IC_{90} (concentrations inhibiting 50% and 90% of parasite viability, respectively) were calculated using GraphPad Prism software 8.0. Selectivity indices (SI) were calculated as the ratio of the CC_{50} to the IC_{50} values. DMSO (≤1%) was used as a negative control. All conditions were performed in duplicate with at least three independent experiments.

4.6 | Reversibility assay

Vero cell cultures infected with *T. cruzi* were treated with the selected coumarin derivatives at concentrations corresponding to 1–2 times the IC_{90} for 10 days at 37°C, following CC_{20} parameters, and were subsequently maintained for an additional 10 days without treatment. The culture medium of both treated and untreated infected cells was replaced every 3–4 days with fresh medium, either with or without the coumarin derivatives. The presence of viable parasites in the culture supernatant was monitored at each medium change by adding D-luciferin (300 μg/mL) and measuring the luminescence using the Glomax microplate reader. At the end of the experiment, both the culture supernatant and cell monolayers were analyzed for parasite viability. Benznidazole (100 μM; Bz), the reference drug, and ≤1% DMSO were used as positive and negative controls,

respectively. At least three independent experiments were performed, with eight to twelve replicates per experiment [21].

4.7 | Statistical Analysis

Data were obtained from at least three independent experiments and are presented as mean ± standard deviation (SD). Statistical analyses were performed using GraphPad Prism software (version 8.0). Data were evaluated utilizing one-way ANOVA followed by Tukey's post hoc test, with a significant threshold of p-value ≤ 0.05.

Acknowledgments

This research was funded by Fundação Oswaldo Cruz, Fundação Carlos Chagas Filho de Amparo à Pesquisa do Estado do Rio de Janeiro (FAPERJ) (grant number E-26/202.409/2021, E26/201.001/2022 and E-26/210.613/2023), Conselho Nacional de Desenvolvimento Científico e Tecnológico (CNPq) (grant number 441649/2024−6 and 404212/2023−9), Fundação Coordenação de Aperfeiçoamento de Pessoal de Nível Superior, Fundação de Amparo à Pesquisa do Estado de Minas Gerais (FAPEMIG; Programa Primeiros Projetos-CEX-APQ-01014−14) and Xunta da Galicia Grant (ED431B 2025/15). The authors thank the Multi-user Research Facility of the Flow Cytometry Platform of Instituto Oswaldo Cruz, Fiocruz, and the Department of Technical Support and Technological Platforms for the facility at Sterilization and Decontamination Centers. We also thank the Coordenação de Aperfeiçoamento de Pessoal de Nível Superior-Brasil (CAPES)-Finance Code 001. Special thanks are extended to Alanderson Nogueira for his technical support. Finally, the authors would like to thank the use of the Mass Spectrometry and Proteomics facilities from Santiago de Compostela University.

Funding

This study was supported by Fundação Oswaldo Cruz, Fundação Carlos Chagas Filho de Amparo à Pesquisa do Estado do Rio de Janeiro (E-26/202.409/2021, E26/201.001/2022, E-26/210.613/2023), Conselho Nacional de Desenvolvimento Científico e Tecnológico (441649/2024-6, 404212/2023-9), Fundação Coordenação de Aperfeiçoamento de Pessoal de Nível Superior, Fundação de Amparo à Pesquisa do Estado de Minas Gerais (Projetos-CEX-APQ-01014-14), Xunta da Galicia (ED431B 2025/15).

Conflicts of Interest

The authors declare no conflicts of interest.

Data Availability Statement

The data that support the findings of this study are available on request from the corresponding author. The data are not publicly available due to privacy or ethical restrictions.

References

1. World Health Organization 2025 Neglected Tropical Diseases, 2025. Assessed on November 18th, https://www.who.int/health-topics/neglected-tropical-diseases#tab=tab_1.

2. K. C. F. Lidani, F. A. Andrade, L. Bavia, et al., "Chagas Disease: From Discovery to a Worldwide Health Problem," *Frontiers in Public Health* 7 (2019): 166.

3. E. Cousin, B. R. Nascimento, J. L. Whisnant et al., "Global, Regional, and National Burden of Chagas Disease, 1990-2023: A Systematic Analysis for the Global Burden of Disease Study 2023 Study Collaborators," *Lancet Infectious Diseases* 26 (2023): 284–301.

4. A. Rassi Jr., A. Rassi, and J. A. Marin-Neto, "Chagas Disease," *Lancet* 375 (2010): 1388–1402.

5. J. A. Pérez-Molina and I. Molina, "Chagas Disease," *Lancet* 391 (2018): 82–94.

6. A. S. de Sousa, D. Vermeij, A. N. Ramos Jr., and A. O. Luquetti, "Chagas Disease," *Lancet* 403 (2024): 203–218.

7. W. M. Schouten, K. Van Bocxlaer, H. Rosing, et al., "Quantitative Analysis of DNDI-6174 Using UPLC-MS/MS: A Preclinical Target Site Pharmacokinetic Study," *Journal of Chromatography B* 1262 (2025): 124652.

8. S. P. S. Rao, M. K. Gould, J. Noeske, et al., "Cyanotriazoles Are Selective Topoisomerase II Poisons that Rapidly Cure Trypanosome Infections," *Science* 380 (2023): 1349–1356.

9. K. Kingwell, "New Therapeutic Candidate for Chagas Disease," *Nature Reviews Drug Discovery* 21 (2022): 796.

10. P. Bosch-Nicolau, M. L. Fernández, E. Sulleiro, et al., "Efficacy of three benznidazole dosing strategies for adults living with chronic Chagas disease (MULTIBENZ): an international, randomised, double-blind, phase 2b trial," *Lancet Infectious Diseases* 24 (2024): 386–394.

11. F. Chappuis, "Oral Fexinidazole for Human African Trypanosomiasis," *Lancet* 391 (2018): 100–102.

12. E. Matovu, W. Nyirenda, A. Eriatu, et al., "Fexinidazole as a New Oral Treatment for Human African Trypanosomiasis due to Trypanosoma Brucei Rhodesiense: A Prospective, Open-Label, Single-Arm, Phase 2–3, Non-Randomised Study," *Lancet Global Health* 13 (2025): e910–e919.

13. F. Torrico, J. Gascón, L. Ortiz, et al., "A Phase 2, Randomized, Multicenter, Placebo-Controlled, Proof-of-Concept Trial of Oral Fexinidazole in Adults With Chronic Indeterminate Chagas Disease," *Clinical Infectious Diseases* 76 (2023): e1186–e1194.

14. M. E. Monteiro, G. Lechuga, L. S. Lara, et al., "Synthesis, Structure-Activity Relationship and Trypanocidal Activity of Pyrazole-Imidazoline and New Pyrazole-Tetrahydropyrimidine Hybrids as Promising Chemotherapeutic Agents for Chagas Disease," *European Journal of Medicinal Chemistry* 182 (2019): 111610.

15. L. M. R. Orlando, G. C. Lechuga, L. S. Lara, et al., "Structural Optimization and Biological Activity of Pyrazole Derivatives: Virtual Computational Analysis, Recovery Assay and 3D Culture Model as Potential Predictive Tools of Effectiveness against Trypanosoma Cruzi," *Molecules* 26 (2021): 6742.

16. E. C. de Oliveira, L. S. Lara, L. M. R. Orlando, et al., "Anti-Trypanosoma Cruzi Potential of New Pyrazole-Imidazoline Derivatives," *Molecules* 30 (2025): 3082.

17. L. M. R. Orlando, L. S. Lara, T. P. de Souza, et al., "Pyrazole-Imidazoline Derivative Prevents Cardiac Damage and Mortality in Acute Trypanosoma Cruzi Infection," *Pharmaceuticals* 18 (2025): 1552.

18. L. S. Lara, G. C. Lechuga, L. M. R. Orlando, et al., "Bioactivity of Novel Pyrazole-Thiazolines Scaffolds against Trypanosoma Cruzi: Computational Approaches and 3D Spheroid Model on Drug Discovery for Chagas Disease," *Pharmaceutics* 14 (2022): 995.

19. V. B. Paes, L. S. Lara, L. M. R. Orlando, et al., "Insights into the Antiparasitic Activity of Pyrazole-Benzimidazole against Trypanosoma Cruzi," *Current Medicinal Chemistry* 32 (2025): 7938–7959.

20. C. N. Pereira, J. O. Rosa, L. S. Lara, et al., "Synthesis by Microwave Irradiation of New Pyrazole-Imidazoline-Pyrimidine Analogs: Physicochemical and Photophysical Properties and Their Biological Activity against Trypanosoma Cruzi," *Journal of Molecular Structure* 1290 (2023): 135899.

21. T. P. de Souza, L. M. R. Orlando, L. S. Lara, et al., "Synthesis and Anti-Trypanosoma Cruzi Activity of New Pyrazole-Thiadiazole Scaffolds," *Molecules* 29 (2024): 3544.

22. J. Pozo-Martínez, F. Salgado, A. Liempi, et al., "Synthesis and Study of the Trypanocidal Activity of Catechol-Containing 3-Arylcoumarins,

Inclusion in β-Cyclodextrin Complexes and Combination with Benznidazole," *Arabian Journal of Chemistry* 15 (2022): 103641.

23. F. Salgado, M. Moncada-Basualto, J. Pozo-Martínez, et al., "Chemical and Biological Analysis of 4-Acyloxy-3-Nitrocoumarins as Trypanocidal Agents," *Arabian Journal of Chemistry* 14 (2021): 102975.

24. N. Robledo-O'Ryan, M. J. Matos, S. Vázquez-Rodríguez, et al., "Synthesis, Antioxidant and Antichagasic Properties of a Selected Series of Hydroxy-3-Arylcoumarins," *Bioorganic & Medicinal Chemistry* 25 (2017): 621–632.

25. A. Muñoz, A. Fonseca, M. J. Matos, et al., "Evaluation of antioxidant and antitrypanosomal properties of a selected series of synthetic 3-carboxamidocoumarins," *ChemistrySelect* 1 (2016): 4957–4964.

26. R. Figueroa Guíñez, M. J. Matos, S. Vázquez-Rodríguez, et al., "Synthesis and Evaluation of Antioxidant and Trypanocidal Properties of a Selected Series of Coumarin Derivatives," *Future Medicinal Chemistry* 5 (2013): 1911–1922.

27. T. Pivetta, S. Masuri, M. G. Cabiddu, et al., "A novel ratiometric and turn-on fluorescent coumarin-based probe for Fe (iii)," *New Journal of Chemistry* 43 (2019): 12032–12041.

28. N. P. Buu-Hoi, G. Saint-Ruf, and B. Lobert, "Oxygen heterocycles. Part XIV. Hydroxylated 3-aryl-and 3-pyridyl-coumarins," *Journal of the Chemical Society C: Organic* 16 (1969): 2069–2070.

29. A. A. de Marchi, M. S. Castilho, P. G. B. Nascimento, et al., "New 3-Piperonylcoumarins as Inhibitors of Glycosomal Glyceraldehyde-3-Phosphate Dehydrogenase (gGAPDH) from Trypanosoma Cruzi," *Bioorganic & Medicinal Chemistry* 12 (2004): 4823–4833.

30. L. M. Kabeya, A. A. de Marchi, A. Kanashiro, et al., "Inhibition of Horseradish Peroxidase Catalytic Activity by New 3-Phenylcoumarin Derivatives: Synthesis and Structure–activity Relationships," *Bioorganic & Medicinal Chemistry* 15 (2007): 1516–1524.

31. I. Molina, J. G. i Prat, F. Salvador, et al., "Randomized Trial of Posaconazole and Benznidazole for Chronic Chagas' Disease," *New England Journal of Medicine* 370 (2014): 1899–1908.

32. C. A. Morillo, H. Waskin, S. Sosa-Estani, et al., "Benznidazole and Posaconazole in Eliminating Parasites in Asymptomatic T. Cruzi Carriers," *Journal of the American College of Cardiology* 69 (2017): 939–947.

33. L. M. MacLean, J. Thomas, M. D. Lewis, et al., "Development of Trypanosoma Cruzi In Vitro Assays to Identify Compounds Suitable for Progression in Chagas' Disease Drug Discovery," *PloS Neglected Tropical Diseases* 12 (2018): e0006612.

34. F. J. Sánchez-Valdéz, A. Padilla, W. Wang, D. Orr, and R. L. Tarleton, "Spontaneous Dormancy Protects Trypanosoma Cruzi during Extended Drug Exposure," *eLife* 7 (2018): e34039.

35. H. Tariq, S. Khan, K. Miyan, et al., "Exploring Natural Coumarins in Antiprotozoal Drug Discovery: A Comprehensive Review," *Chemistry & Biodiversity* 22 (2025): e01964.

36. S. Valencia, W. Quiñones, S. Robledo, J. C. Marín-Loaiza, D. Durango, and J. Gil, "Antiparasitic Activity of Coumarin–Chalcone (3-Cinnamoyl-2 *H* -Chromen-2-Ones) Hybrids," *Chemistry & Biodiversity* 22 (2025): e202402515.

37. J. A. Nunes, F. N. da Silva, E. B. da Silva, et al., "Coumarin-based derivatives targeting Trypanosoma cruzi cruzain and Trypanosoma brucei cathepsin L-like proteases," *New Journal of Chemistry* 47 (2023): 10127–10146.

38. S. H. Cemali, S. Poyraz, S. Belveren, et al., "Recent Insights in Multi-Target Drugs in Pharmacology and Medicinal Chemistry," *ChemMedChem* 20 (2025): e202500447.

39. A. M. Silber, R. R. Tonelli, C. G. Lopes, et al., "Glucose Uptake in the Mammalian Stages of Trypanosoma Cruzi," *Molecular and Biochemical Parasitology* 168 (2009): 102–108.

40. M. B. Alencar, S. Marsiccobetre, A. C. Mengarda, M. S. Ballari, A. M. Silber, and M. Rodrigues, "Energy Metabolism in *Trypanosoma Cruzi* : the Validated and Putative Bioenergetic and Carbon Sources," *mBio* 16 (2025): e02215–e02224.

41. C. Henriques, A. Henriques-Pons, M. Meuser-Batista, A. S. Ribeiro, and W. de Souza, "In Vivo Imaging of Mice Infected with Bioluminescent Trypanosoma Cruzi Unveils Novel Sites of Infection," *Parasites & Vectors* 7 (2014): 89.

Supporting Information

Additional supporting information can be found online in the Supporting Information section.